JACS
JOURNAL OF THE AMERICAN CHEMICAL SOCIETY
pubs.acs.org/JACS
Article

End-to-End Distance Probability Distributions of Dilute Poly(ethylene oxide) in Aqueous Solution

Nicholas Sherck, Thomas Webber, Dennis Robinson Brown, Timothy Keller, Mikayla Barry, Audra DeStefano, Sally Jiao, Rachel A. Segalman, Glenn H. Fredrickson, M. Scott Shell,* and Songi Han*

Cite This: J. Am. Chem. Soc. 2020, 142, 19631−19641

Read Online

ACCESS | Metrics & More | Article Recommendations | Supporting Information

ABSTRACT: We introduce a powerful, widely applicable approach to characterizing polymer conformational distributions, specifically the end-to-end distance distributions, $P(R_{ee})$, accessed through double electron−electron resonance (DEER) spectroscopy in conjunction with molecular dynamics (MD) simulations. The technique is demonstrated on one of the most widely used synthetic, disordered, water-soluble polymers: poly(ethylene oxide) (PEO). Despite its widespread importance, no systematic experimental characterization of PEO's R_{ee} conformational landscape exists. The evaluation of $P(R_{ee})$ is particularly important for short polymers or (bio)polymers with sequence complexities that deviate from simple polymer physics scaling laws valid for long chains. In this study, we characterize the R_{ee} landscape by measuring $P(R_{ee})$ for low molecular weight (MW: 0.22−2.6 kDa) dilute PEO chains. We use DEER with end-conjugated spin probes to resolve R_{ee} populations from ∼2−9 nm and compare them with full distributions from MD. The $P(R_{ee})$'s from DEER and MD show remarkably good agreement, particularly at longer chain lengths where populations in the DEER-unresolvable range (<1.5 nm) are low. Both the $P(R_{ee})$ and the root-mean-square $\tilde{R}_{ee}$ indicate that aqueous PEO is a semiflexible polymer in a good solvent, with the latter scaling linearly with molecular weight up to its persistence length ($l_p \sim 0.48$ nm), and rapidly transitioning to excluded volume scaling above l_p. The $\tilde{R}_{ee}$ scaling is quantitatively consistent with that from experimental scattering data on high MW (>10 kDa) PEO and the $P(R_{ee})$'s crossover to the theoretical distribution for an excluded volume chain.

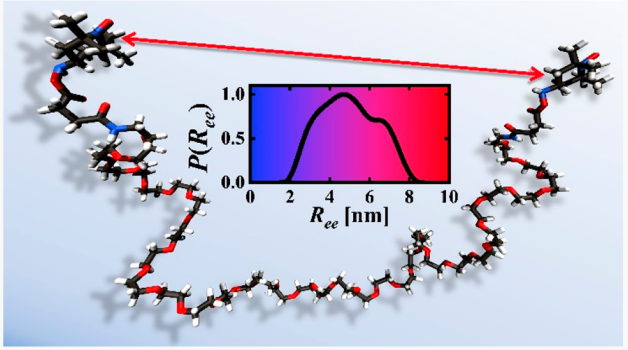

INTRODUCTION

Poly(ethylene oxide) (PEO) is one of the most widely studied and used polymers, with applications ranging from biomedicine, consumer products, and antifouling coatings to membrane technologies.[1−3] PEO's utility is in large part due to its high hydrophilicity stemming from the spacing and conformations of the backbone ether oxygens that integrate into water's hydrogen-bonding network.[4,5] PEO is structurally a simple polymer comprised of one repeat unit, [−CH_2−O−CH_2−], terminated by either [−CH_3] or [−OH]. If terminated by an alcohol, then it is conventionally known as polyethylene glycol (PEG), and if terminated by methyl groups, then it is known as PEO, though we will refer to both as PEO throughout this work. Although the repeat unit of PEO is structurally simple, PEO has a complex interaction with water that depends on temperature, molecular weight, and concentration, exhibiting both lower and upper critical solution temperatures with a resulting closed-loop, temperature-density phase diagram with a molecular weight dependence.[6,7] This complex phase behavior stems from the intricate, temperature-dependent balance between ether−water and water−water hydrogen bonding.[8,9] The local interplay of water along the chain backbone directly affects PEO's conformations and modulates its solubility in water.

While PEO is widely studied as a water-soluble polymer, its complex behavior in water suggests a diverse conformational landscape that remains incompletely understood. Here "landscape" indicates the ensemble of conformations sampled by a highly disordered and fluctuating polymer. The distribution of PEO's end-to-end distance, R_{ee}, provides one insight into this landscape, with a rich connection to theories of polymer physics, but this distribution has not been investigated experimentally. Understanding the nature of the conformational landscape is especially important for studies of short polymer chains, which show deviations from asymptotic

Received: August 12, 2020
Published: November 3, 2020

https://dx.doi.org/10.1021/jacs.0c08709
J. Am. Chem. Soc. 2020, 142, 19631−19641

polymer scaling laws. Moreover, beyond PEO, there is significant interest in understanding deviations from scaling theories for more complicated polymers with heterogeneous sequences, such as intrinsically disordered proteins. Yet generally, the distribution of conformational states is difficult to obtain due to the limited suite of experimental techniques that can directly characterize the full ensemble of conformers. Traditional scattering techniques are well-suited for looking at global polymer length scales between *all* scattering sites in a system,[10] but they lack direct information about more finely resolved correlations, such as distances between specific sites, including polymer ends, or of defined pairs of residues across a protein.

Our work addresses polymer end-to-end distance ensembles by directly measuring and computing the end-to-end distance distribution, $P(R_{ee})$, of dilute PEO. Specifically, we characterize PEO's $P(R_{ee})$ by using both double electron−electron resonance (DEER) spectroscopy and molecular dynamics (MD) simulations. Coupling DEER and MD enables a significantly more detailed understanding of PEO's R_{ee} conformational landscape, a level of detail that has remained largely inaccessible using prior experimental or simulation techniques alone. While the present work addresses PEO as an important model system, this combined approach should offer insights into a wide range of other disordered polymers.

Prior experimental investigations of PEO probe averages of the underlying conformational landscape, such as the average radius-of-gyration, R_g, or the average hydrodynamic radius, R_h, but do not detail the *ensemble* of conformational states, as accessed by $P(R_{ee})$. Data on PEO for average R_g and R_h from scattering and size-exclusion chromatography experiments cover a broad molecular weight regime (~300−1.1 × 10^6 Da).[11−22] Most of these studies focus on high molecular weight chains (greater than ~10 kDa, 35 data points), with few on low molecular weight PEO's (greater than ~10 kDa, 9 data points).[16,18−20,23,24] The lack of data for short chains is likely due to the increased difficulty in obtaining a reliable scattering signal for chains with small characteristic dimensions (i.e., R_g ~ 1 nm). From these data, there is a strong consensus that long-chain PEO behaves as a polymer in good solvent (i.e., an excluded volume polymer).

Complementary to scattering methods, experimental techniques based on "spectroscopic rulers" provide nanoscopic information about the local structure of molecules by tethering probes to sites of interest. The two most common techniques are fluorescence resonance energy transfer (FRET) and DEER. FRET is relatively well-established and widely used for the structural characterization of biomolecules, providing site-specific information between 2 and 10 nm by measuring the energy exchange between fluorophores conjugated to target sites.[25−28] FRET detects the fluorophores' average separation and hence is most successfully used in cases where binary changes in macromolecular conformations exist (e.g., folded vs unfolded, open vs closed protein states, or isolated vs assembled states).[29−31] Only with the addition of single-molecule detection (smFRET) can information about the *distribution* of distances of an ensemble of polymer conformations be obtained, though the potential impact of the large fluorophores on FRET distances must be taken into account.[32] As an example of the conformational effect of fluorophores, small-angle X-ray scattering (SAXS) data for R_g indicates that water is a good solvent for many chemically denatured proteins that do not show conformational changes with varying denaturant concentration (e.g., guanidine hydrochloride, GuHCl, or urea between 1 and 8 M); however, FRET measurements using dye-labeled variants of the denatured proteins (e.g., protein L;[33,34] CspTm 1−66,[35] 2−66,[36] and 1−54;[37] HIV-1 integrase;[37] ProTaC;[37] IM7 17−70, leqm17−56, 17−56, and 36−70;[38] and Im9)[39] register an expansion in the mean interdye distance with increasing denaturant concentration.[40] Interestingly, the same discrepancy exists for aqueous PEO.[20,32,41−43] Both Watkins et al. and Qu et al. used smFRET to characterize aqueous PEO at varying denaturant (urea or GuHCl) concentrations, finding an *increase* in interdye distances (for Watkins, an ~10% increase) with increasing denaturant concentration.[40,43] Riback et al. attributed the disagreement to the chain-end labeled fluorophores that enhance chain compaction upon labeling, arising from fluorophore−fluorophore and fluorophore−chain interactions.[32] Importantly, none of these smFRET studies on PEO convert the smFRET histograms to a $P(R_{ee})$ of the interdye distances; rather they report a single descriptor of the underlying conformational landscape (e.g., typically the mean or most likely R_{ee} value).

DEER is an experimental characterization method capable of resolving not only mean distances but also the full distance distributions between spin probes.[44,45] As a pulsed electron paramagnetic resonance (EPR) technique, DEER uses the dipole−dipole interaction between two paramagnetic centers and the subsequent spin interaction relaxations to probe intramolecular distance distributions reliably between 2 and 9 nm.[46] DEER has now been used for a wide range of structural biology applications (e.g., to determine intraprotein distances, to resolve multiple conformational states, to determine the structure of large protein complexes by triangulating interprotein distances, or to study the transitions between structured (folded) and unstructured (unfolded) states of biomolecules).[44,47−51] Surprisingly, there are relatively fewer applications of DEER to examine and extract information from the full $P(R_{ee})$ distribution and even fewer $P(R_{ee})$ studies of *synthetic* polymer conformations.[52−54] In fact, the primary advantage of DEER as a spectroscopic ruler is that it directly yields the complete distance distribution of the macromolecular ensemble. Additional benefits of DEER include that the spin-probes are significantly smaller than FRET fluorophores (~2−3 times smaller diameters), and are identical on both ends, whereas FRET requires two distinct fluorophores, complicating the labeling process.[55,56] The small spin probes available with DEER are advantageous for small and conformationally flexible macromolecules (e.g., low-molecular-weight PEO) where large probes overwhelm the conformational states of the small polymers.

As with FRET, DEER has short distance limitations that are a result of (1) the length of the pump pulse exceeding the duration of the dipolar oscillation for short wavelengths;[57] (2) finite bandwidth limitations when a significant portion of the distance population is below 2 nm;[46] and (3) the breakdown in the underlying assumption of negligible exchange coupling below 1.5 nm.[44,58] It is interesting to note that below 2 nm, continuous wave (cw) EPR is a technique complementary to DEER that can determine mean distances and distributions between 1 and 2 nm by assessing dipole−dipole couplings from spectral line broadening.[46] At long distances, the DEER restrictions are less severe, and the maximum resolvable distance is largely dictated by the decoherence time of the dipolar signal before the echo intensity is lost in the

https://dx.doi.org/10.1021/jacs.0c08709
J. Am. Chem. Soc. 2020, 142, 19631−19641

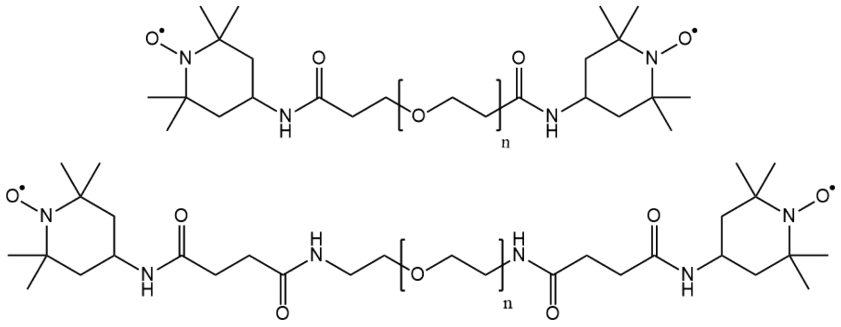

Figure 1. Spin-labeled PEO chemistries in this study. The series of PEO lengths is n = 5, 13, and 25 for the upper structure, and n = 36 and 59 for the lower structure.

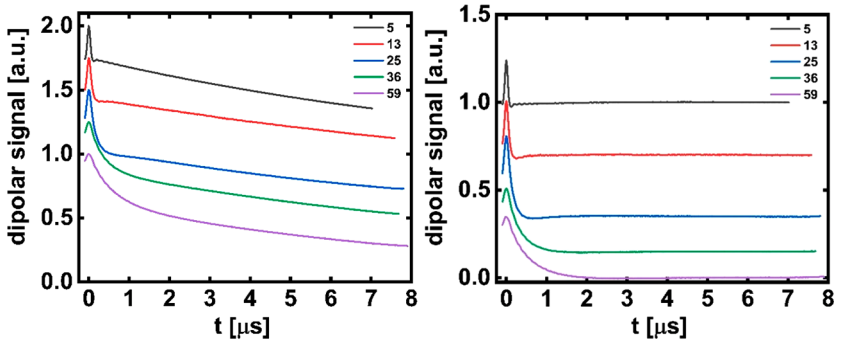

Figure 2. Time domain dipolar signal $V(t)$ from DEER experiments for PEO chains with 5, 13, 25, 36, and 59 monomers (220−2600 Da) shifted vertically for clarity (left). Background-corrected (dimensionality = 3) dipolar signal of the same (right).

background noise. Norman and co-workers have shown that deuteration of not only the solvent but also the macromolecule can dramatically lengthen the decoherence time of the DEER echo signal and hence allows the accessible distance to be extended up to ∼14 nm.[59,60] Further details on the limitations of DEER are described in Supporting Information section 2a.

Complementary to both the smFRET and DEER techniques are MD simulations, increasingly used to enhance signal analysis by providing atomic resolution.[29,41,42,46,61,62] Several atomistic force-fields (FF) have been shown to nicely capture different properties (structural or thermodynamic) of aqueous PEO, depending on target properties during their parametrization;[63−71] excellent comparisons of the current atomistic PEO FFs have been given by Laaksonen and colleagues, Maginn and co-workers, and Sadowski and colleagues.[63,64,67] Among recently successful models for simulating both PEO and water are the second-generation General AMBER FF (GaFF2) and the newer 4-site Optimal Point Charge (OPC4) water model.[72,73] GaFF was originally developed by Wang et al. for small molecules, and recently underwent a major reparameterization, including improved Lennard-Jones (LJ) parameters.[74,84] The updated ether parameters reflect the changes proposed by Barbosa et al. to improve the original GaFF for neat 2- to 5-mer PEO oligomers. Their work developed LJ parameters that capture neat PEO oligomer densities (within a few percent relative error), dielectric constants, thermal expansivities, enthalpies of vaporization, and conformer populations.[63,75]

In this work, we utilize DEER spectroscopy and MD simulations concurrently to characterize PEO's R_{ee} conformational landscape by reporting detailed probability distributions of R_{ee}, $P(R_{ee})$. We demonstrate that this combined approach is a powerful means to assess the states of the conformational ensemble of disordered macromolecules. This also represents the first experimental study that directly probes the $P(R_{ee})$ of PEO in water and enables detailed comparisons to polymer physics theories for the molecular weight scaling of the average, root-mean-square R_{ee} ($\tilde{R}_{ee}$), as well as to the full $P(R_{ee})$ distributions. In the "Methods" section we discuss the experimental and simulation protocols used to extract the $P(R_{ee})$'s. We present in the "Results" section the $P(R_{ee})$'s from DEER and simulation and our investigation of the $\tilde{R}_{ee}$ molecular weight scaling and its comparison to the available literature data, followed by a detailed comparison to the theoretical $P(R_{ee})$ from asymptotic polymer physics valid in the high molecular weight limit, and close with a discussion of the higher-order moments of the distributions. In the Discussion, we comment on two topics of debate in the literature about aqueous PEO: (1) whether or not there is an intermediary, ideal scaling regime in the $\tilde{R}_{ee}$ before the asymptotic, excluded volume scaling characteristic of high molecular weight chains and (2) whether or not PEO has a helical structure in water.

METHODS

Spin-Labeling of PEO. We purchased two variants of PEO for spin-labeling. The three smallest PEO chains (5-, 13-, and 25-mer) are from BroadPharm (Bis-PEG-NHS ester), and the two largest (36- and 59-mer) are from Sigma-Aldrich (*O*,*O*′-bis[2-(*N*-succinimidyl-succinylamino)ethyl]polyethylene glycol), Figure 1. GPC analysis determined that the polydispersity index of the 36- and 59-mer were 1.017 and 1.015, respectively, Supporting Information section 1a. We spin labeled both variants of PEO in the same manner, by dissolving NHS functionalized PEO in THF, followed by addition of a molar excess (∼10-fold) of 4-amino-2,2,6,6-tetramethylpiperidine-1-oxyl (4-amino-TEMPO), Supporting Information section 1c. We purified the largest three PEO variants (25-, 36-, and 59-mers) using a 1 kDa dialysis membrane (Spectra/Por 7 Dialysis Membranes, 1 kDa

https://dx.doi.org/10.1021/jacs.0c08709
J. Am. Chem. Soc. 2020, 142, 19631−19641

MWCO) in DI water, with five solution exchanges, twice per day. We purified the smallest two oligomers (5- and 13-mers) using liquid column chromatography with 9:1 dichloromethane/methanol as the mobile phase and silica gel as the stationary phase. We lyophilized each sample after purification to produce a fine, white powder. NMR analysis verified the presence of PEO ether peaks in each sample (Supporting Information section 1d).

Experimental Double-Electron Electron Resonance (DEER). The samples contained 100 μM spin-labeled PEO in D_2O, with 30% by volume deuterated glycerol added as a cryoprotectant. We added approximately 40 μL of sample to a 3 mm OD, 2 mm ID quartz capillary that was flash-frozen in liquid nitrogen before performing DEER. Flash freezing is necessary for DEER experiments, and the rapid cooling preserves polymer conformations.[76,77] We performed DEER experiments with a pulsed Q-band Bruker E580 Elexsys spectrometer, equipped with a Bruker QT-II resonator and a 300 W TWT amplifier (Applied Systems Engineering, Model 177 Ka); see Figure 2 for the raw DEER signal traces. We maintained the temperature at 60 K using a Bruker/ColdEdge FlexLine Cryostat (Model ER 4118HV-CF100). We applied the following four-pulse DEER sequence to all samples: $\pi_{obs}/2-\tau_1-\pi_{obs}-(t-\pi_{pump})-(\tau_2-t)-\pi_{obs}-\tau_2-$echo. Optimized observer pulses based on a nutation measurement were approximately 20 ns for 90 pulses and 40 ns for 180 pulses. We applied a linear chirp π_{pump} pulse with a length of 100 ns and a frequency width of 80 MHz. The observed frequency was 90 MHz higher than the center of the pump frequency range. τ_1 was 180 ns, and τ_2 was set to 8 μs. We acquired the time-domain data with 16 ns time resolution in 500 increments up to 8 μs dipolar evolution time and ran the DEER experiment with signal averaging for ~12 h. The time-domain DEER signal, $V(t)$, was baseline-corrected using a model with dimensionality of three. Finding the solution for $P(R_{ee})$ from $V(t)$ is a well-known ill-posed inversion problem. Here, we relied on the "model-free" Tikhonov regularization method with non-negativity constraints to reconstruct $P(R_{ee})$ using the LongDistances software.[78] The Tikhonov regularization approach is chosen as it is the most widely used approach to calculate $P(R_{ee})$ from high-quality DEER data, especially when $P(R_{ee})$ is uniformly broad and non-Gaussian. The development of more robust approaches to find solutions for $P(R_{ee})$ is an active area of research, which include a global Gaussian model fitting approach,[79] Srivastava–Freed Truncated Singular Value Decomposition (SF-TSVD),[80,81] the use of Bayesian statistics to determine uncertainty,[82] or a global parameter-free distribution approach by DEERLab,[83] to name a few prominent approaches. However, for the type of DEER data at hand in this study, the solutions for $P(R_{ee})$ by Tikhonov regularization with a carefully chosen regularization parameter are robust (Supporting Information section 2b).

Molecular Dynamics (MD) Simulations. We use the second-generation General Amber FF (GaFF2) for the MD simulations, a classical, fixed-charged FF that allows for parametrization of a wide variety of organic molecules.[75,84] We assign fixed point charges to the TEMPO spin label and PEO using the Gaussian '16 software package and the RESP charge fitting implemented in AmberTools.[85,86] We use the B3LYP functional and the 6-311++G(d,p) basis set, which has been shown to work well for assigning RESP charges to Glymes.[63,85] We also include results for AM1-BCC charging, a semiempirical quantum calculation, on the unlabeled PEO to access the results' sensitivity to charging. The details of the charge assignment and the charges sensitivity to the level of theory can be found in the Supporting Information section 3.

We conduct simulations of dilute (single chain), spin-labeled PEO chains of varying length—between 1 (46 Da) and 59 (2.6 kDa) monomeric units in an aqueous solvent (4-site OPC water model) at 300 K.[73] We use the OpenMM package on Nvidia P100 and V100 GPUs.[87] To ensure system equilibration before collecting data, we perform simulations in stages (details in Supporting Information section 4): (1) energy minimization of the initial structure generated using Packmol,[88] (2) *NVT* annealing at elevated temperature, 500 K, (3) *NVT* cooldown to 298 K, (4) *NPT* equilibration at 298 K, and; (5) *NVT* production at 298 K (volume fixed to the average calculated from the prior *NPT* equilibration step). We collect atomic coordinates every 10 ps and postsimulation analyze the trajectories to obtain thermodynamic and structural property averages (both TEMPO labeled and unlabeled) using decorrelated samples.

We analyze the simulation data using a custom Python analysis script along with the MDTraj Python library.[89] We calculate the end-to-end distance, R_{ee}, either from the two oxygen radicals (on the spin probes) or from the terminal carbons on the PEO-backbones; throughout, we report the average, *root-mean-square* $\langle R_{ee}^2\rangle^{1/2}$ and $\langle R_g^2\rangle^{1/2}$ values, notated simply as $\tilde{R}_{ee}$ and $\tilde{R}_g$. A standard, percentile bootstrap analysis is used on the P_{ee}'s to estimate the uncertainty in the distributions.[90] We calculate the persistence length by fitting a decaying exponential to the ensemble-averaged, bond–bond (between oxygens along the PEO backbone) orientational correlation function between bond vectors $\boldsymbol{b}_i$ and $\boldsymbol{b}_{i+m}$:

$$C_{bb}(m) = \left\langle \frac{\boldsymbol{b}_i \cdot \boldsymbol{b}_{i+m}}{|\boldsymbol{b}_i||\boldsymbol{b}_{i+m}|} \right\rangle \sim C_o\, e^{-mb/l_p};\ m \in \{0, n_b - 1\} \quad (1)$$

where n_b is the number of bonds in the chain (in the case of the oxygen–oxygen bond vectors, it is the number of monomers less one), b is the average bond–bond vector (ensemble-averaged along the entire chain), and l_p is the characteristic length scale of the decay, interpreted here as the persistence length.[91,92]

RESULTS

End-to-End Distributions. We study the end-to-end distances of aqueous PEO chains in the molecular weight range of 220–2600 Da (5- to 59-mer). We perform DEER on spin-labeled PEO to obtain the R_{ee} distance distributions, $P(R_{ee})$, as a function of molecular weight. The time-domain dipolar signal $V(t)$ derived from DEER (Figure 2 (left)) is baseline-corrected (Figure 2 (right)), and the $P(R_{ee})$ is reconstructed by Tikhonov regularization (see the "Methods" section). DEER analysis and reconstruction methods are discussed in Supporting Information section 2b. The modulation depth for the DEER-derived $V(t)$ signal is 0.34 on average, and a dipolar evolution time up to 8 μs is used. The signal-to-noise ratio is exceptionally high (1340 on average). We find robust solutions to $P(R_{ee})$ distributions, given the high-quality $V(t)$ data (Figure 3 (top)). The resulting $P(R_{ee})$ is representative of the ensemble average conformations of all PEO chains in solution and their respective R_{ee} distances. The position of $P(R_{ee})$ readily distinguishes the different molecular weight PEOs studied, with the maximum peak position in $P(R_{ee})$ moving to larger distances as the chain length grows.

At a higher molecular weight, the shape of $P(R_{ee})$ becomes less sharp and broadens, that is, the chain and its ends experience greater conformational freedom as the polymer length increases beyond the persistence length (l_p). However, due to the chain conformational entropy, the probability of finding R_{ee} separations beyond the average are penalized. For shorter, more rigid chains, the decay is rapid, while for the longer, more flexible ones the decay is less severe, with detectable chain-end excursion to larger separations, resulting in a long-ranged, decaying tail. From polymer physics models of $P(R_{ee})$, the appearance of the long-ranged, decaying tail is expected because the characteristic decay length is related to $\langle R_{ee}^2\rangle^{1/2}$, at least in the asymptotic, high molecular weight limit. The observed broadening from a more peaked to a more diffuse $P(R_{ee})$ is indicative of a semiflexible polymer in a good solvent, in which the polymer chain is swollen by excluded volume interactions as the molecular weight increases. The DEER data indicate that as PEO increases in length in a good

https://dx.doi.org/10.1021/jacs.0c08709
J. Am. Chem. Soc. 2020, 142, 19631–19641

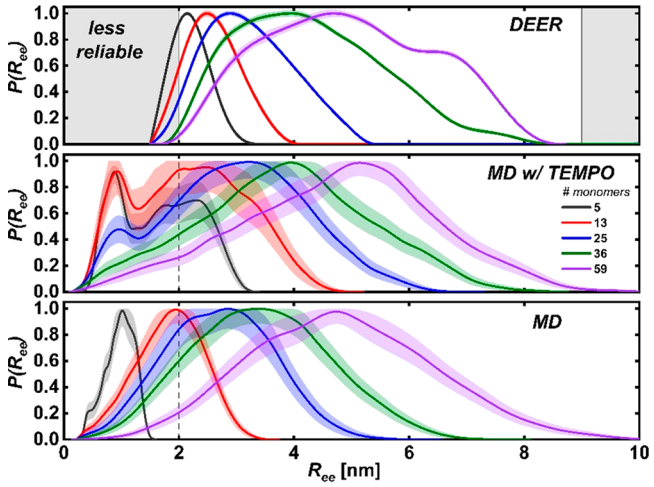

Figure 3. End-to-end distance probability distributions, $P(R_{ee})$, normalized by their respective maximums for PEO chains with 5, 13, 25, 36, and 59 monomers (220−2600 Da). (top) Results from DEER spectroscopy measurements with ±2 standard deviations represented by shaded regions around the lines. The light gray shaded regions indicate where the DEER measurements are less reliable, <2 and >9 nm. (middle) MD simulation results for PEO chains with TEMPO spin labels on the ends. The R_{ee} distance is taken to be that between the radical oxygens on the TEMPO groups; see Figure 1. (bottom) MD simulation results for PEO chains without TEMPO spin labels. The R_{ee} distance is taken to be that between the last carbons on the PEO chain. For both sets of simulation results, the shaded regions around the lines represent ±1 standard deviation.

solvent (i.e., water), beyond l_p it adopts a diffuse structure. This is contrary to the behavior expected of a poor solvent associated with chains adopting a compact structure. While these are well-known polymer physics features for a model disordered polymer in good solvent, they have not been observed experimentally as viewed from direct measurements of $P(R_{ee})$.

While DEER measurements can resolve $P(R_{ee})$ between 2 and 9 nm with a high level of accuracy, there is growing uncertainty in the tails, mainly at small separations, as discussed in the introduction.[46] In this case, simulations are complementary and informative. Here, we conduct MD simulations on *single* aqueous PEO chains of identical lengths and with TEMPO spin labels (Figure 3, middle), with the R_{ee} defined as the distance between the radical oxygen on each probe. As with the DEER $P(R_{ee})$, the MD distributions show an expanding R_{ee} conformational space with increasing molecular weight. Again, a prominent and growing tail on the high end of the distribution exists, as is expected for a polymer in good solvent. In fact, the high-end tail in $P(R_{ee})$ for all chain lengths is quantitatively consistent with those from the DEER measurements.

MD distributions show a significant population at short distances, most notably in the region below 2 nm, which DEER spectroscopy cannot resolve (see Supporting Information section 2a for a detailed description of contributing factors). Specifically, the MD $P(R_{ee})$ reveals a peak at 1 nm Figure 3 (middle) that corresponds to a hydrophobic attraction between the largely apolar spin labels, where they associate so that the radical oxygens are 1 nm apart. Even unlabeled PEO end-group chemistry influences end aggregation in water; in fact, the aggregation is stronger for the more hydrophobic, CH_3-terminated chains (PEO) than for OH-terminated chains (PEG).[93−96] Importantly, however, the spin labels do not seem to affect the shape of $P(R_{ee})$ relative to the DEER data at larger separations, as can be seen in Figure 3.

The perturbation arising from spin label aggregation and the probability of observing short R_{ee} separations diminish rapidly with increasing molecular weight, resulting in growing qualitative (Figure 3, top and middle panels) and quantitative agreement (Supporting Information section 5) between simulations and experiments. For comparison, we perform simulations on PEO without spin labels, Figure 3 (bottom), which lack the 1 nm peak due to end aggregation. This observation implies that the probes do not simply offset the average R_{ee}'s to higher values and increase their variances, at least for the shortest chains, but slightly bias the chain statistics due to their propensity to end-aggregate. We estimate the probe aggregation strength to be on the order of ~0.7 k_bT by comparing $P(R_{ee})$s from the labeled and unlabeled MD simulations (Supporting Information section 6). Because this attraction is comparable to the thermal energy, for short chains with a low conformational entropy, a clear population of conformations exists in which the chain ends interact, possibly in a transient bound state. However, Jacobson−Stockmayer (JS) theory predicts a strong molecular weight dependence for

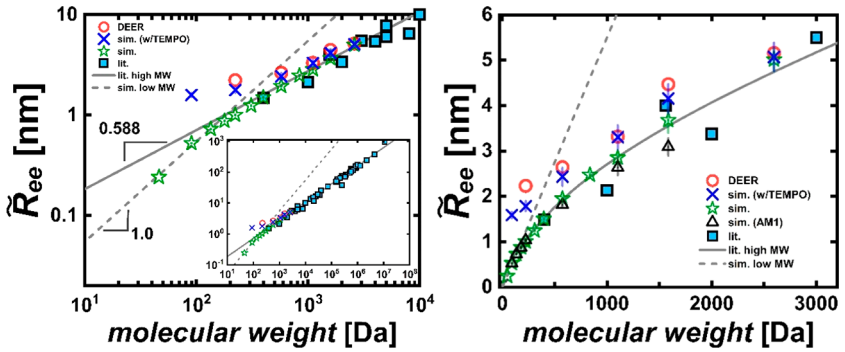

Figure 4. Scaling of $\tilde{R}_{ee}$ from both DEER spectroscopy and MD simulations compared to prior literature data from various scattering experiments (light and neutron); see Supporting Information section 7b for details.[11−20] The solid, gray line is a power−law fit to the relation for excluded volume scaling, $\tilde{R}_{ee} = a(\mathrm{MW})^{\nu}$, where $\nu = 0.588$ and $a = 0.047(4)$ nm. The dashed, gray line is a power law fit to our simulations of unlabeled PEO, with the exponent fixed to 1. Left: log−log plot of $\tilde{R}_{ee}$ covering the entire range of available data. Right: linear plot of the data focusing on the low-molecular-weight regime. Simulation results for the semiempirical, quantum calculation, AM1-BCC (AM1), are also shown, black triangles. ±1 standard error is shown for $\tilde{R}_{ee}$ simulation values.

https://dx.doi.org/10.1021/jacs.0c08709
J. Am. Chem. Soc. 2020, 142, 19631−19641

the probability of chain cyclization (i.e., ends close enough to react), showing that it scales as $MW^{-\tau}$ (for a Gaussian chain, $\tau = 3/2$).[97] Indeed, the aggregation peak at 1 nm (Figure 3, middle) is strongly molecular-weight-dependent, decreasing rapidly for chains longer than the 13-mer. We also examine the fractional error in $\tilde{R}_{ee}$ between both DEER and MD with the probes to the MD results without them and note at least a $\tau \sim 3/2$ scaling per JS theory (Supporting Information section 5), resulting from the decreased contribution from short R_{ee} distances to $P(R_{ee})$.

Root-Mean-Square R_{ee}: $\tilde{R}_{ee}$. The full polymer R_{ee} distributions carry an immense amount of information (e.g., spin-label aggregation). However, the distribution's second moment, $\langle R_{ee}^2 \rangle = \tilde{R}_{ee}^2$, can be directly compared to universal polymer scaling predictions of the form:

$$\tilde{R}_{ee} = a(MW)^{\nu} \quad (2)$$

The prefactor, a, is a chemistry-dependent quantity, while the scaling exponent, ν, depends on solvent quality. For a theta solvent, $\nu = 0.5$ (ideal scaling), while for good solvents $\nu \sim 0.588$ (excluded volume scaling).[98,99]

Figure 4 compares $\tilde{R}_{ee}$ values from both DEER measurements and MD simulations to high molecular weight values extracted from light- and neutron-scattering experiments in the literature. The literature data is compiled as follows, with details in Supporting Information sections 7b and 8. We use nonlinear, least-squares regression to fit the literature-obtained, high molecular weight, $\tilde{R}_g$ scattering data to eq 2 with a fixed excluded volume exponent ($\nu = 0.588$), finding $a = 0.047(4)$ nm; for details, see Supporting Information section 7b. To convert the literature $\tilde{R}_g$ scaling to $\tilde{R}_{ee}$, we use the asymptotic relation: $\tilde{R}_{ee}^2 = 6.25\tilde{R}_g^2$ (6 for an ideal chain).[98] Supporting Information section 8 compares literature and simulation $\tilde{R}_g$ values against molecular weight. Where possible, neutron-scattering data is compiled from the literature for low molecular weight PEO chains (<10 kDa, Supporting Information section 7b). However, there is relatively less data for the low molecular weight regime examined in this study (<2.6 kDa) and a large variation within the available literature data (Figure 4; right, blue squares). In all, the literature data set covers several decades of PEO molecular weight data (300−10^8 Da), and shows a clear asymptotic excluded volume scaling regime (Figure 4; left, solid line).

Importantly, both the DEER and MD data from the present study show excellent convergence at higher molecular weights to the literature-derived excluded volume scaling (Figure 4). Although expected, the convergence of the DEER data is notable, as this technique directly probes R_{ee}, while scattering studies directly probe $\tilde{R}_g$, for which the proportionality constant relating it to $\tilde{R}_{ee}$ is only known in the limit of infinitely long chains. Thus, observing the crossover represents both experimental confirmation of this relation and the efficacy of the DEER technique to probe intramolecular correlations. Moreover, the TEMPO-labeled $\tilde{R}_{ee}$ data from both DEER and MD are in excellent agreement past the 13-mer, with no fit parameters in the simulation model. Even the subtle uptick in $\tilde{R}_{ee}$ at the 36-mer (1.6 kDa) resulting from use of a longer linker between the polymer and the spin probe for the 36-mer and longer chains (Figure 1) is detected in both DEER and MD. The quantitative agreement between DEER and MD for the TEMPO-labeled chains at or above ∼576 Da (13-mer) again emphasizes the validity of the simulation force fields for PEO, TEMPO, and water.

The simulations without the TEMPO spin labels also cross over rapidly to the literature scaling (Figure 4, solid gray line) as the chain increases in length beyond l_p. As a further check of the scaling behavior, we also fit the unlabeled simulation data (MW ≥ 576 Da, $n = 5$) to eq 2, allowing both a and ν to float (Supporting Information section 9). We find a scaling exponent consistent with excluded volume interactions, $\nu = 0.62 \pm 0.01$, with 99% confidence intervals that encompass the scaling result from the literature scattering data; see Figure S20 A. In contrast, for the shortest chains comparable to or below l_p, $\tilde{R}_{ee}$ scales linearly, $\nu = 1$, with molecular weight denoted by the dashed line in Figure 4. This regime is only present for chains of ∼3 monomers or less, consistent with PEO's flexibility; its l_p is on the order of 0.47−0.55 nm as estimated from single-molecule, force spectroscopy experiments.[100,101] We estimate the simulation PEO model to have l_p of 0.484 ± 0.001 nm, in good agreement; details about calculating the persistence length as well as results for Flory's characteristic ratio (C_n) can be found in Supporting Information section 10.

We investigate the role of the PEO force field and find that the method of assignment of atomic partial charges can produce distinct $\tilde{R}_{ee}$ scaling behavior. Specifically, we find that the charges from the B3LYP calculation give good agreement with experimental results, performing significantly better than the less-polar PEO model using AM1 calculated charges. The AM1 charges degrease l_p by 6% to 0.450 ± 0.005 nm, which noticeably impacts longer chains; see the 36-mer in Figure 4 (right, black triangles). The observed difference is directly related to the solvent−polymer interaction, as B3LYP results in larger partial charge magnitudes and enhances the ether backbone's hydrogen-bonding with water (see Supporting Information section 11 for $O_w - O_{EO}$ and $H_w - O_{EO}$ radial distribution functions, and number of O_w and H_w per monomer), resulting in a more rigid polymer and a larger l_p.

We also use the simulation data to calculate the ratio of $\tilde{R}_{ee}^2/\tilde{R}_g^2$ ($\alpha^2 \equiv \tilde{R}_{ee}^2/\tilde{R}_g^2$, Supporting Information section 13), to provide insight into the shape of the polymer in solution. An α value of 2 indicates a sphere, while larger values indicate increasingly prolate ellipsoids, moving toward a value of 3.46 for a cylindrical rod. In between are polymers for which theory predicts $\alpha = 2.45$ for a theta-solvent (ideal, Gaussian chain statistics) and $\alpha = 2.5$ for a good solvent (excluded volume chain statistics). For the unlabeled chains, we observe a rapid rise in α from ∼2 for a single monomer, essentially a thin, rigid rod with ends laying on a sphere, to a maximum of ∼2.7 near l_p (Supporting Information section 13), indicating a more cylindrical shape due to stiffness along the chain backbone (i.e., a semiflexible polymer). Beyond the maximum, α approaches 2.5 from above, consistent with excluded volume scaling for polymers much longer than l_p (∼600−1000 Da), although there is too much uncertainty in the data to assess this definitively.

Scaled End-to-End Distributions. The fully resolved distributions from experiment and simulation allow us to make a detailed assessment of PEO's conformational landscape in comparison to polymer theory for $P(R_{ee})$ in the asymptotic, high molecular weight limit. The theoretical prediction for the functional form of $P(R_{ee})$ uses an interpolation between the low- and high-r limits, colloquially known as des Cloizeaux's scaling form:[98]

$$P(x) = P(R_{ee})\tilde{R}_{ee} = a_1 x^{\varepsilon_1} \exp(-a_2 x^{\varepsilon_2}) 4\pi x^2 \quad (3)$$

https://dx.doi.org/10.1021/jacs.0c08709
J. Am. Chem. Soc. 2020, 142, 19631−19641

where x is the scaled end-to-end distance ($x = R_{ee}/\tilde{R}_{ee}$ where $\tilde{R}_{ee} \equiv \langle R_{ee}^2 \rangle^{1/2}$), $4\pi x^2$ accounts for the radial degeneracy, and ε_1 and ε_2 are 0.269 and 2.427 for an excluded volume chain (versus 0 and 2 for an ideal chain). The normalization condition and second moment constraint ($\langle R_{ee}^2 \rangle = 4\pi \int R_{ee}^4 P(R_{ee})\, dR_{ee}$) require $a_1 = 0.299$ and $a_2 = 1.269$ for an excluded volume chain (0.33 and 1.5 for an ideal chain).

We show $P(x)$ in Figure 5 from DEER and simulation, observing that they both approach the excluded volume result

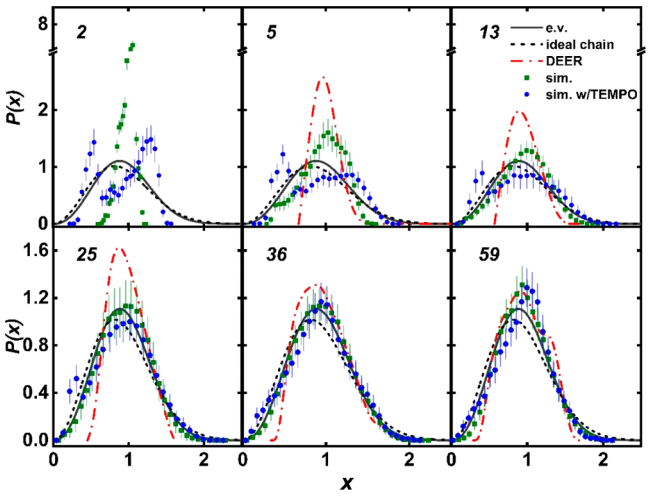

Figure 5. End-to-end distance probability distributions scaled by the average, root-mean-square, end-to-end distance, $\tilde{R}_{ee}P(R_{ee})$, for 2, 5, 13, 25, 36, and 59 monomers. The solid and dashed lines are the universal distributions for excluded volume (e.v.) and ideal chains, respectively.[98,101] Error bars are ±1 standard deviation.

(Figure 5, solid black line) as the chain length increases. However, the experimental and the spin-labeled simulation results approach from different directions. The DEER measurements asymptote by broadening as the molecular weight increases, though remaining consistently narrower across all lengths; we attribute this dampened broadening to limitations in resolving short distances, which is most apparent for the low molecular weight PEO chains (5-, 13-, and 25-mer) where simulations show spin-label aggregation. However, the labeled MD distributions approach the asymptotic form by narrowing, as probe aggregation becomes increasingly less important with growing molecular weight. The unlabeled MD distributions approach excluded volume scaling within simulation error, with a decreasing signature of residual stiffness, a narrow, sharply peaked distribution, as molecular weight increases beyond the persistence length.

Higher-Order Moments. Higher-order central moments of the scaled distributions in Figure 5 provide further quantitative descriptors of universal polymer scaling behavior. Figure 6 reports the variance (σ^2) and skewness (μ^3), describing the distribution's width and symmetry around the mean, respectively (see Supporting Information section 14 for the kurtosis (μ^4)). It is important to note that higher-order moments put increasingly more emphasis on the tail regions of the distributions; these are the regions in both DEER and MD associated with the greatest sources of error from sampling and inherent biases.

We find excellent asymptotic, long-chain agreement between DEER and MD estimates of the distribution variance and skewness and, through the simulations, are able to pinpoint

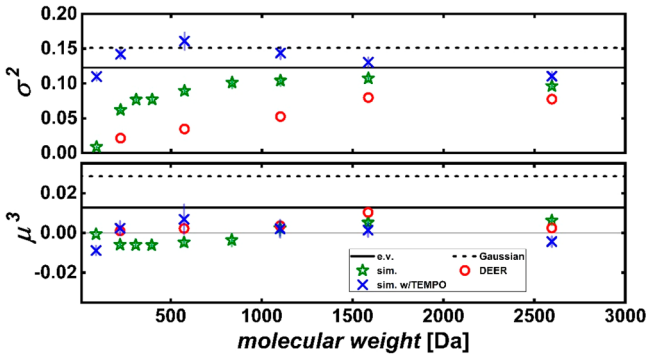

Figure 6. Second and third moments of the scaled, end-to-end distance probability distributions in Figure 5. The solid and dashed lines are the moments numerically calculated from the universal distributions for ev and ideal Gaussians chains, respectively. Error bars are ±1 standard deviation.

small spin-label effects present only for short chains. The variance, which characterizes the magnitude of R_{ee} fluctuations and hence the diversity of the conformational ensemble, increases with molecular weight for both the DEER and unlabeled MD results; however, for short chains the DEER-measured variance is smaller, which as discussed originates from its inability to probe distances below ~2 nm. The labeled MD simulations, in contrast, show a nonmonotonic behavior, owing to the weak probe-aggregation at distances below ~2 nm. The skewness is nearly zero for all DEER and MD measurements, showing a weak if any preference for chain excursions to longer lengths relative to the average, and more consistent with excluded volume polymer scaling than that of an ideal chain.

DISCUSSION

The present experimental and simulation results support the picture that short PEO oligomers are stiff objects that grow linearly up to l_p (~100 Da), then quickly transition over to the characteristic excluded volume scaling of a polymer in a good solvent, consistent with literature experimental scattering data. However, some literature studies suggest that dilute, PEO chains exhibit ideal scaling (i.e., $\nu = 0.5$) up to a molecular weight of 1600 Da, based on measured hydrodynamic radii (R_h), single-molecule elasticity measurements, and molecular simulations.[18,100,102,103] Polymer theory does allow for an intermediate, ideal scaling regime if the thermal blob size, ξ_T, is greater than l_p, where ξ_T is the length scale at which excluded volume interactions begin to swell the polymer chain.[104] However, the R_h scaling ought to be interpreted cautiously, as R_h is known to yield an effective scaling exponent, ν_h, that is smaller than the true ν.[98] Single-molecule elasticity measurements, while providing high-quality data, rely on scaling theories to estimate the crossover boundaries, often not accounting for proportionality constants that prevent a precise comparison. In the present study, it is possible that buried in the narrow transition regime (~100−600 Da) in Figure 4 **is** an ideal scaling regime that is more finely resolved in single-molecule force spectroscopy measurements.[100,105] Furthermore, several prior simulation efforts for aqueous PEO using other force fields (Supporting Information sections 7 and 8) find systematically lower $\tilde{R}_{ee}$ and $\tilde{R}_g$ compared to both our data and the literature scattering data; their scaling more closely resembles the less polar, AM1-charged PEO model, suggesting

https://dx.doi.org/10.1021/jacs.0c08709
J. Am. Chem. Soc. 2020, 142, 19631−19641

poorer solvent quality (i.e., a smaller ν), which could reveal an expanded intermediate, ideal scaling regime. Nevertheless, scaling from both our data and the literature scattering data indicate that excluded volume scaling is reached for chains above ~600 Da. This scaling also agrees with experimentally measured second virial coefficients for aqueous PEO chains in the range of 600−10 000 Da using a freezing point depression technique reported by Wang et al.[106]

A persistent topic of discussion in the literature is whether PEO adopts a helical conformation in water.[16,105] Our data suggest that the PEO backbone does show weak helicity but only locally along the chain. Specifically, our simulations of PEO ranging from dimers up to a 59-mer reveal a significant fraction (~30%) of −C−O−C−C−O−C− dihedral sequences that are trans−gauche−trans (tgt) in water (Supporting Information section 12), which is the preferred sequence of PEO's strongly helical crystal structure.[107,108] Thus, in water the disordered PEO shows remnants of the preferred sequencing in the crystalline state; however, given its remarkable flexibility in solution, reflected by its small l_p, these helical segments are weakly correlated. These observations might explain the seemingly inconsistent data of both Oesterhelt and Alessi insofar that it is difficult to detect such weak structural correlations and that aqueous PEO's flexibility allows for chains of any reasonable length (our data suggest chains $\gtrsim$1.1 kDa (25-mer) are in the excluded volume regime) to adopt chain conformations consistent with an excluded volume coil, even in the presence of locally helical backbone conformations.[109]

CONCLUSION

Using DEER spectroscopy in conjunction with MD simulations, we provide a detailed picture of the end-to-end distance conformational landscape of dilute, aqueous PEO, a model semiflexible, disordered synthetic polymer, reporting full $P(R_{ee})$'s for the ensemble of chain structures in the molecular weight range of 0.22−2.6 kDa. We find excellent agreement between the DEER and MD $P(R_{ee})$'s, both of which reveal similar trends and increasingly quantitative agreement as the chain length grows, while providing a compelling argument that PEO behaves as an excluded volume polymer. The root-mean-square, average end-to-end distance, $\tilde{R}_{ee}$, from both DEER and MD approaches the asymptotic, excluded volume scaling of the literature scattering data from high molecular weight PEO chains. Moreover, we find that the shape of the measured and simulated $P(R_{ee})$s for the longest chains compare favorably to the theoretical distribution for an excluded volume chain. We find that the effect of the spin labels on the polymer conformations drops off rapidly with chain length. Overall, we believe the combination of DEER and simulation to be a powerful approach, together able to provide detailed information about the rich conformational landscapes of macromolecules and their specific intramolecular correlations.

ASSOCIATED CONTENT

Supporting Information

The Supporting Information is available free of charge at https://pubs.acs.org/doi/10.1021/jacs.0c08709.

PEO sample preparation, polydispersity, and NMR characterization; DEER limitations and data analysis; descriptions of molecular simulation force fields, water models, and simulation protocols; demonstration of spin probe aggregation and effect of spin probe on R_{ee} trends; R_{ee} correlation times; PEO R_g values from simulation and comparison to literature models; PEO persistence length and Flory's characteristic ratio from simulation; R_{ee} trend with molecular weight fits; description of the radial distribution functions and water hydration; dihedral populations; scaled distributions; and the ratio, $\alpha = \tilde{R}_{ee}^2/\tilde{R}_g^2$ (PDF)

AUTHOR INFORMATION

Corresponding Authors

M. Scott Shell − *Department of Chemical Engineering, University of California, Santa Barbara, California 93106, United States;* orcid.org/0000-0002-0439-1534; Email: shell@ucsb.edu

Songi Han − *Department of Chemical Engineering and Department of Chemistry and Biochemistry, University of California, Santa Barbara, California 93106, United States;* orcid.org/0000-0001-6489-6246; Email: songi@chem.ucsb.edu

Authors

Nicholas Sherck − *Department of Chemical Engineering, University of California, Santa Barbara, California 93106, United States;* orcid.org/0000-0001-5503-1494

Thomas Webber − *Department of Chemical Engineering, University of California, Santa Barbara, California 93106, United States*

Dennis Robinson Brown − *Department of Chemical Engineering, University of California, Santa Barbara, California 93106, United States*

Timothy Keller − *Department of Chemistry and Biochemistry, University of California, Santa Barbara, California 93106, United States*

Mikayla Barry − *Department of Materials, University of California, Santa Barbara, California 93106, United States*

Audra DeStefano − *Department of Chemical Engineering, University of California, Santa Barbara, California 93106, United States*

Sally Jiao − *Department of Chemical Engineering, University of California, Santa Barbara, California 93106, United States*

Rachel A. Segalman − *Department of Chemical Engineering and Department of Materials, University of California, Santa Barbara, California 93106, United States;* orcid.org/0000-0002-4292-5103

Glenn H. Fredrickson − *Department of Chemical Engineering, Department of Materials, and Materials Research Laboratory, University of California, Santa Barbara, California 93106, United States;* orcid.org/0000-0002-6716-9017

Complete contact information is available at: https://pubs.acs.org/10.1021/jacs.0c08709

Notes

The authors declare no competing financial interest.

ACKNOWLEDGMENTS

This research was primarily supported by the Center for Materials for Water and Energy Systems (M-WET), an Energy Frontier Research Center funded by the US Department of Energy (DOE), Office of Science, Basic Energy Sciences (BES), under award no. DE-SC0019272. Resources for the

computational studies were provided by the Center for Scientific Computing at the CNSI and supported by the MRL under NSF grant no. CNS-1725797 and NSF MRSEC grant no. DMR1720256. S.J. acknowledge support from NSF Graduate Research Fellowships (DGE 1650114), and M.B. recognizes support from the Office of Naval Research (ONR) under award no. N00014-17-1-2047. The authors gratefully acknowledge helpful discussions with T. Casey, J. Monroe, C. Altenbach, G. Jeschke, and K. Tsay.

REFERENCES

(1) D'souza, A. A.; Shegokar, R. Polyethylene Glycol (PEG): A Versatile Polymer for Pharmaceutical Applications. *Expert Opin. Drug Delivery* **2016**, *13* (9), 1257−1275.
(2) Kang, G.; Cao, Y. Development of Antifouling Reverse Osmosis Membranes for Water Treatment: A Review. *Water Res.* **2012**, *46* (3), 584−600.
(3) Padaki, M.; Surya Murali, R.; Abdullah, M. S.; Misdan, N.; Moslehyani, A.; Kassim, M. A.; Hilal, N.; Ismail, A. F. Membrane Technology Enhancement in Oil−Water Separation. A Review. *Desalination* **2015**, *357*, 197−207.
(4) Wada, R.; Fujimoto, K.; Kato, M. Why Is Poly(Oxyethylene) Soluble in Water? Evidence from the Thermodynamic Profile of the Conformational Equilibria of 1,2-Dimethoxyethane and Dimethoxymethane Revealed by Raman Spectroscopy. *J. Phys. Chem. B* **2014**, *118* (42), 12223−12231.
(5) Ensing, B.; Tiwari, A.; Tros, M.; Hunger, J.; Domingos, S. R.; Pérez, C.; Smits, G.; Bonn, M.; Bonn, D.; Woutersen, S. On the Origin of the Extremely Different Solubilities of Polyethers in Water. *Nat. Commun.* **2019**, *10* (1), 2893.
(6) Bae, Y. C.; Lambert, S. M.; Soane, D. S.; Prausnitz, J. M. Cloud-Point Curves of Polymer Solutions from Thermooptical Measurements. *Macromolecules* **1991**, *24* (15), 4403−4407.
(7) Saeki, S.; Kuwahara, N.; Nakata, M.; Kaneko, M. Upper and Lower Critical Solution Temperatures in Poly (Ethylene Glycol) Solutions. *Polymer* **1976**, *17* (8), 685−689.
(8) Bekiranov, S.; Bruinsma, R.; Pincus, P. Solution Behavior of Polyethylene Oxide in Water as a Function of Temperature and Pressure. *Phys. Rev. E: Stat. Phys., Plasmas, Fluids, Relat. Interdiscip. Top.* **1997**, *55* (1), 577.
(9) Dormidontova, E. E. Role of Competitive PEO−Water and Water−Water Hydrogen Bonding in Aqueous Solution PEO Behavior. *Macromolecules* **2002**, *35* (3), 987−1001.
(10) Bergmann, A.; Fritz, G.; Glatter, O. Solving the Generalized Indirect Fourier Transformation (GIFT) by Boltzmann Simplex Simulated Annealing (BSSA). *J. Appl. Crystallogr.* **2000**, *33* (5), 1212−1216.
(11) Devanand, K.; Selser, J. C. Asymptotic Behavior and Long-Range Interactions in Aqueous Solutions of Poly(Ethylene Oxide). *Macromolecules* **1991**, *24* (22), 5943−5947.
(12) Kawaguchi, S.; Imai, G.; Suzuki, J.; Miyahara, A.; Kitano, T.; Ito, K. Aqueous Solution Properties of Oligo- and Poly(Ethylene Oxide) by Static Light Scattering and Intrinsic Viscosity. *Polymer* **1997**, *38* (12), 2885−2891.
(13) Stuart, M. A. C.; Waajen, F. H. W. H.; Cosgrove, T.; Vincent, B.; Crowley, T. L. Hydrodynamic Thickness of Adsorbed Polymer Layers. *Macromolecules* **1984**, *17* (9), 1825−1830.
(14) Le Coeur, C.; Teixeira, J.; Busch, P.; Longeville, S. Compression of Random Coils Due to Macromolecular Crowding: Scaling Effects. *Phys. Rev. E* **2010**, *81* (6), No. 061914.
(15) Polverari, M.; van de Ven, T. G. M. Dilute Aqueous Poly(Ethylene Oxide) Solutions: Clusters and Single Molecules in Thermodynamic Equilibrium. *J. Phys. Chem.* **1996**, *100* (32), 13687−13695.
(16) Alessi, M. L.; Norman, A. I.; Knowlton, S. E.; Ho, D. L.; Greer, S. C. Helical and Coil Conformations of Poly(Ethylene Glycol) in Isobutyric Acid and Water. *Macromolecules* **2005**, *38* (22), 9333−9340.
(17) Rubinson, K. A.; Hubbard, J. Experimental Compressibilities and Average Intermolecular Distances of Poly(Ethylene Glycol) Molecular Masses 2000−8000 Da in Aqueous Solution. *Polymer* **2009**, *50* (12), 2618−2623.
(18) Petrenko, V.; Bulavin, L.; Avdeev, M.; Garamus, V.; Koneracka, M.; Kopcansky, P. Structure and Interaction of Poly(Ethylene Glycol) in Aqueous Solutions. Small-Angle Neutron Scattering Data. *Macromol. Symp.* **2014**, *335* (1), 20−23.
(19) Lancz, G.; Avdeev, M. V.; Petrenko, V. I.; Garamus, V. M.; Koneracká, M.; Kopčanský, P. SANS Study of Poly(Ethylene Glycol) Solutions in D_2O. *Acta Phys. Pol., A* **2010**, *118* (5), 980−982.
(20) Watkins, H. M.; Simon, A. J.; Sosnick, T. R.; Lipman, E. A.; Hjelm, R. P.; Plaxco, K. W. Random Coil Negative Control Reproduces the Discrepancy between Scattering and FRET Measurements of Denatured Protein Dimensions. *Proc. Natl. Acad. Sci. U. S. A.* **2015**, *112* (21), 6631−6636.
(21) Kuga, S. Pore Size Distribution Analysis of Gel Substances by Size Exclusion Chromatography. *Journal of Chromatography A* **1981**, *206* (3), 449−461.
(22) Hammouda, B.; Ho, D. L. Insight into Chain Dimensions in PEO/Water Solutions. *J. Polym. Sci., Part B: Polym. Phys.* **2007**, *45* (16), 2196−2200.
(23) Le Cœur, C.; Combet, S.; Carrot, G.; Busch, P.; Teixeira, J.; Longeville, S. Conformation of the Poly(Ethylene Glycol) Chains in DiPEGylated Hemoglobin Specifically Probed by SANS: Correlation with PEG Length and in Vivo Efficiency. *Langmuir* **2015**, *31* (30), 8402−8410.
(24) Rubinson, K. A.; Krueger, S. Poly(Ethylene Glycol)s 2000−8000 in Water May Be Planar: A Small-Angle Neutron Scattering (SANS) Structure Study. *Polymer* **2009**, *50* (20), 4852−4858.
(25) Deniz, A. A.; Dahan, M.; Grunwell, J. R.; Ha, T.; Faulhaber, A. E.; Chemla, D. S.; Weiss, S.; Schultz, P. G. Single-Pair Fluorescence Resonance Energy Transfer on Freely Diffusing Molecules: Observation of Forster Distance Dependence and Subpopulations. *Proc. Natl. Acad. Sci. U. S. A.* **1999**, *96* (7), 3670−3675.
(26) Beechem, J. M.; Haas, E. Simultaneous Determination of Intramolecular Distance Distributions and Conformational Dynamics by Global Analysis of Energy Transfer Measurements. *Biophys. J.* **1989**, *55* (6), 1225−1236.
(27) Stryer, L.; Haugland, R. P. Energy Transfer: A Spectroscopic Ruler. *Proc. Natl. Acad. Sci. U. S. A.* **1967**, *58* (2), 719.
(28) Schuler, B.; Soranno, A.; Hofmann, H.; Nettels, D. Single-Molecule FRET Spectroscopy and the Polymer Physics of Unfolded and Intrinsically Disordered Proteins. *Annu. Rev. Biophys.* **2016**, *45* (1), 207−231.
(29) Schuler, B.; Lipman, E. A.; Steinbach, P. J.; Kumke, M.; Eaton, W. A. Polyproline and the "Spectroscopic Ruler" Revisited with Single-Molecule Fluorescence. *Proc. Natl. Acad. Sci. U. S. A.* **2005**, *102* (8), 2754.
(30) Selvin, P. R. The Renaissance of Fluorescence Resonance Energy Transfer. *Nat. Struct. Biol.* **2000**, *7* (9), 730−734.
(31) Holmes, B. B.; Furman, J. L.; Mahan, T. E.; Yamasaki, T. R.; Mirbaha, H.; Eades, W. C.; Belaygorod, L.; Cairns, N. J.; Holtzman, D. M.; Diamond, M. I. Proteopathic Tau Seeding Predicts Tauopathy in Vivo. *Proc. Natl. Acad. Sci. U. S. A.* **2014**, *111* (41), E4376−E4385.
(32) Riback, J. A.; Bowman, M. A.; Zmyslowski, A. M.; Plaxco, K. W.; Clark, P. L.; Sosnick, T. R. Commonly Used FRET Fluorophores Promote Collapse of an Otherwise Disordered Protein. *Proc. Natl. Acad. Sci. U. S. A.* **2019**, *116* (18), 8889.
(33) Merchant, K. A.; Best, R. B.; Louis, J. M.; Gopich, I. V.; Eaton, W. A. Characterizing the Unfolded States of Proteins Using Single-Molecule FRET Spectroscopy and Molecular Simulations. *Proc. Natl. Acad. Sci. U. S. A.* **2007**, *104* (5), 1528−1533.
(34) Sherman, E.; Haran, G. Coil−Globule Transition in the Denatured State of a Small Protein. *Proc. Natl. Acad. Sci. U. S. A.* **2006**, *103* (31), 11539−11543.
(35) Lipman, E. A.; Schuler, B.; Bakajin, O.; Eaton, W. A. Single-Molecule Measurement of Protein Folding Kinetics. *Science* **2003**, *301* (5637), 1233−1235.

https://dx.doi.org/10.1021/jacs.0c08709
J. Am. Chem. Soc. 2020, 142, 19631−19641

(36) Schuler, B.; Lipman, E. A.; Eaton, W. A. Probing the Free-Energy Surface for Protein Folding with Single-Molecule Fluorescence Spectroscopy. *Nature* **2002**, *419* (6908), 743−747.
(37) Müller-Späth, S.; Soranno, A.; Hirschfeld, V.; Hofmann, H.; Rüegger, S.; Reymond, L.; Nettels, D.; Schuler, B. Charge Interactions Can Dominate the Dimensions of Intrinsically Disordered Proteins. *Proc. Natl. Acad. Sci. U. S. A.* **2010**, *107* (33), 14609.
(38) Pugh, S. D.; Gell, C.; Smith, D. A.; Radford, S. E.; Brockwell, D. J. Single-Molecule Studies of the Im7 Folding Landscape. *J. Mol. Biol.* **2010**, *398* (1), 132−145.
(39) Tezuka-Kawakami, T.; Gell, C.; Brockwell, D. J.; Radford, S. E.; Smith, D. A. Urea-Induced Unfolding of the Immunity Protein Im9Monitored by SpFRET. *Biophys. J.* **2006**, *91* (5), L42−L44.
(40) Watkins, H. M.; Simon, A. J.; Sosnick, T. R.; Lipman, E. A.; Hjelm, R. P.; Plaxco, K. W. Random Coil Negative Control Reproduces the Discrepancy between Scattering and FRET Measurements of Denatured Protein Dimensions. *Proc. Natl. Acad. Sci. U. S. A.* **2015**, *112* (21), 6631−6636.
(41) Zheng, W.; Borgia, A.; Buholzer, K.; Grishaev, A.; Schuler, B.; Best, R. B. Probing the Action of Chemical Denaturant on an Intrinsically Disordered Protein by Simulation and Experiment. *J. Am. Chem. Soc.* **2016**, *138* (36), 11702−11713.
(42) Fuertes, G.; Banterle, N.; Ruff, K. M.; Chowdhury, A.; Mercadante, D.; Koehler, C.; Kachala, M.; Estrada Girona, G.; Milles, S.; Mishra, A.; Onck, P. R.; Gräter, F.; Esteban-Martín, S.; Pappu, R. V.; Svergun, D. I.; Lemke, E. A. Decoupling of Size and Shape Fluctuations in Heteropolymeric Sequences Reconciles Discrepancies in SAXS vs. FRET Measurements. *Proc. Natl. Acad. Sci. U. S. A.* **2017**, *114* (31), E6342.
(43) Qu, S.; Liu, C.; Liu, Q.; Wu, W.; Du, B.; Wang, J. Solvent Effect on FRET Spectroscopic Ruler. *J. Chem. Phys.* **2018**, *148* (12), 123331.
(44) Jeschke, G. DEER Distance Measurements on Proteins. *Annu. Rev. Phys. Chem.* **2012**, *63* (1), 419−446.
(45) Fajer, P. G.; Brown, L.; Song, L. Practical Pulsed Dipolar ESR (DEER). *ESR Spectrosc. Membr. Biophys.* **2007**, *27*, 95−128.
(46) Banham, J. E.; Baker, C. M.; Ceola, S.; Day, I. J.; Grant, G. H.; Groenen, E. J. J.; Rodgers, C. T.; Jeschke, G.; Timmel, C. R. Distance Measurements in the Borderline Region of Applicability of CW EPR and DEER: A Model Study on a Homologous Series of Spin-Labelled Peptides. *J. Magn. Reson.* **2008**, *191* (2), 202−218.
(47) Kaminker, R.; Kaminker, I.; Gutekunst, W. R.; Luo, Y.; Lee, S.; Niu, J.; Han, S.; Hawker, C. J. Tuning Conformation and Properties of Peptidomimetic Backbones through Dual N/Cα-Substitution. *Chem. Commun.* **2018**, *54* (41), 5237−5240.
(48) Morimoto, J.; Fukuda, Y.; Kuroda, D.; Watanabe, T.; Yoshida, F.; Asada, M.; Nakamura, T.; Senoo, A.; Nagatoishi, S.; Tsumoto, K.; Sando, S. A Peptoid with Extended Shape in Water. *J. Am. Chem. Soc.* **2019**, *141* (37), 14612−14623.
(49) Van Eps, N.; Altenbach, C.; Caro, L. N.; Latorraca, N. R.; Hollingsworth, S. A.; Dror, R. O.; Ernst, O. P.; Hubbell, W. L. Gi- and Gs-Coupled GPCRs Show Different Modes of G-Protein Binding. *Proc. Natl. Acad. Sci. U. S. A.* **2018**, *115* (10), 2383−2388.
(50) Segawa, T. F.; Doppelbauer, M.; Garbuio, L.; Doll, A.; Polyhach, Y. O.; Jeschke, G. Water Accessibility in a Membrane-Inserting Peptide Comparing Overhauser DNP and Pulse EPR Methods. *J. Chem. Phys.* **2016**, *144* (19), 194201.
(51) Schiemann, O.; Weber, A.; Edwards, T. E.; Prisner, T. F.; Sigurdsson, S. T. Nanometer Distance Measurements on RNA Using PELDOR. *J. Am. Chem. Soc.* **2003**, *125* (12), 3434−3435.
(52) Bücker, D.; Sickinger, A.; Ruiz Perez, J. D.; Oestringer, M.; Mecking, S.; Drescher, M. Direct Observation of Chain Lengths and Conformations in Oligofluorene Distributions from Controlled Polymerization by Double Electron−Electron Resonance. *J. Am. Chem. Soc.* **2020**, *142* (4), 1952−1956.
(53) Godt, A.; Schulte, M.; Zimmermann, H.; Jeschke, G. How Flexible Are Poly(Para-Phenyleneethynylene)s? *Angew. Chem., Int. Ed.* **2006**, *45* (45), 7560−7564.
(54) Hintze, C.; Schütze, F.; Drescher, M.; Mecking, S. Probing of Chain Conformations in Conjugated Polymer Nanoparticles by Electron Spin Resonance Spectroscopy. *Phys. Chem. Chem. Phys.* **2015**, *17* (48), 32289−32296.
(55) Chiang, Y.-W.; Borbat, P. P.; Freed, J. H. The Determination of Pair Distance Distributions by Pulsed ESR Using Tikhonov Regularization. *J. Magn. Reson.* **2005**, *172* (2), 279−295.
(56) Banham, J. E.; Timmel, C. R.; Abbott, R. J. M.; Lea, S. M.; Jeschke, G. The Characterization of Weak Protein−Protein Interactions: Evidence from DEER for the Trimerization of a von Willebrand Factor A Domain in Solution. *Angew. Chem., Int. Ed.* **2006**, *45* (7), 1058−1061.
(57) Doll, A.; Qi, M.; Godt, A.; Jeschke, G. CIDME: Short Distances Measured with Long Chirp Pulses. *J. Magn. Reson.* **2016**, *273*, 73−82.
(58) Schweiger, A.; Jeschke, G. *Principles of Pulse Electron Paramagnetic Resonance*; Oxford University Press, 2001.
(59) El Mkami, H.; Norman, D. G. EPR Distance Measurements in Deuterated Proteins. *Methods Enzymol.* **2015**, *564*, 125−152.
(60) Ward, R.; Bowman, A.; Sozudogru, E.; El-Mkami, H.; Owen-Hughes, T.; Norman, D. G. EPR Distance Measurements in Deuterated Proteins. *J. Magn. Reson.* **2010**, *207* (1), 164−167.
(61) Polyhach, Y.; Bordignon, E.; Jeschke, G. Rotamer Libraries of Spin Labelled Cysteines for Protein Studies. *Phys. Chem. Chem. Phys.* **2011**, *13* (6), 2356−2366.
(62) Sezer, D.; Freed, J. H.; Roux, B. Simulating Electron Spin Resonance Spectra of Nitroxide Spin Labels from Molecular Dynamics and Stochastic Trajectories. *J. Chem. Phys.* **2008**, *128* (16), 165106−165106.
(63) Barbosa, N. S. V.; Zhang, Y.; Lima, E. R. A.; Tavares, F. W.; Maginn, E. J. Development of an AMBER-Compatible Transferable Force Field for Poly(Ethylene Glycol) Ethers (Glymes). *J. Mol. Model.* **2017**, *23* (6), 194.
(64) Wang, Y.-L.; Lawrence, R. S.; Lu, Z.-Y.; Laaksonen, A. Molecular Dynamics Study of Aqueous Solution of Polyethylene Oxide: Critical Test of Force Field Models. *Soft Mater.* **2013**, *11* (4), 371−383.
(65) Lee, H.; Venable, R. M.; MacKerell, A. D.; Pastor, R. W. Molecular Dynamics Studies of Polyethylene Oxide and Polyethylene Glycol: Hydrodynamic Radius and Shape Anisotropy. *Biophys. J.* **2008**, *95* (4), 1590−1599.
(66) Anderson, P. M.; Wilson, M. R. Developing a Force Field for Simulation of Poly(Ethylene Oxide) Based upon *Ab Initio* Calculations of 1,2-Dimethoxyethane. *Mol. Phys.* **2005**, *103* (1), 89−97.
(67) Fischer, J.; Paschek, D.; Geiger, A.; Sadowski, G. Modeling of Aqueous Poly(Oxyethylene) Solutions: 1. Atomistic Simulations. *J. Phys. Chem. B* **2008**, *112* (8), 2388−2398.
(68) Fischer, J.; Paschek, D.; Geiger, A.; Sadowski, G. Modeling of Aqueous Poly(Oxyethylene) Solutions. 2. Mesoscale Simulations. *J. Phys. Chem. B* **2008**, *112* (43), 13561−13571.
(69) Barbosa, N. S. V.; Zhang, Y.; Lima, E. R. A.; Tavares, F. W.; Maginn, E. J. Development of an AMBER-Compatible Transferable Force Field for Poly(Ethylene Glycol) Ethers (Glymes). *J. Mol. Model.* **2017**, *23* (6), 194.
(70) Oh, S. Y.; Yang, H. E.; Bae, Y. C. Molecular Simulations and Thermodynamic Modeling for Closed-Loop Phase Miscibility of Aqueous PEO Solutions. *Macromol. Res.* **2013**, *21* (8), 921−930.
(71) Smith, G. D.; Yoon, D. Y.; Jaffe, R. L.; Colby, R. H.; Krishnamoorti, R.; Fetters, L. J. Conformations and Structures of Poly(Oxyethylene) Melts from Molecular Dynamics Simulations and Small-Angle Neutron Scattering Experiments. *Macromolecules* **1996**, *29* (10), 3462−3469.
(72) Onufriev, A. V.; Izadi, S. Water Models for Biomolecular Simulations. *Wiley Interdisciplinary Reviews: Computational Molecular Science* **2018**, *8* (2), e1347.
(73) Izadi, S.; Anandakrishnan, R.; Onufriev, A. V. Building Water Models: A Different Approach. *J. Phys. Chem. Lett.* **2014**, *5* (21), 3863−3871.
(74) Wang, J. The second generation of the general AMBER force field I: van der Waals parameterization. **2017**, manuscript in preparation.

https://dx.doi.org/10.1021/jacs.0c08709
J. Am. Chem. Soc. 2020, 142, 19631−19641

(75) Wang, J.; Wolf, R. M.; Caldwell, J. W.; Kollman, P. A.; Case, D. A. Development and Testing of a General Amber Force Field. *J. Comput. Chem.* **2004**, *25* (9), 1157−1174.
(76) Ruthstein, S.; Potapov, A.; Raitsimring, A. M.; Goldfarb, D. Double Electron Electron Resonance as a Method for Characterization of Micelles. *J. Phys. Chem. B* **2005**, *109* (48), 22843−22851.
(77) Georgieva, E. R.; Roy, A. S.; Grigoryants, V. M.; Borbat, P. P.; Earle, K. A.; Scholes, C. P.; Freed, J. H. Effect of Freezing Conditions on Distances and Their Distributions Derived from Double Electron Electron Resonance (DEER): A Study of Doubly-Spin-Labeled T4 Lysozyme. *J. Magn. Reson.* **2012**, *216*, 69−77.
(78) Altenbach, C. *LongDistances*; 2019.
(79) Brandon, S.; Beth, A. H.; Hustedt, E. J. The Global Analysis of DEER Data. *J. Magn. Reson.* **2012**, *218*, 93−104.
(80) Srivastava, M.; Freed, J. H. Singular Value Decomposition Method to Determine Distance Distributions in Pulsed Dipolar Electron Spin Resonance. *J. Phys. Chem. Lett.* **2017**, *8* (22), 5648−5655.
(81) Srivastava, M.; Freed, J. H. Singular Value Decomposition Method To Determine Distance Distributions in Pulsed Dipolar Electron Spin Resonance: II. Estimating Uncertainty. *J. Phys. Chem. A* **2019**, *123* (1), 359−370.
(82) Edwards, T. H.; Stoll, S. A Bayesian Approach to Quantifying Uncertainty from Experimental Noise in DEER Spectroscopy. *J. Magn. Reson.* **2016**, *270*, 87−97.
(83) Fábregas Ibáñez, L.; Jeschke, G.; Stoll, S. DeerLab: A Comprehensive Toolbox for Analyzing Dipolar EPR Spectroscopy Data. *Magnetic Resonance Discussions* **2020**, *1*, 209−224.
(84) Case, D. A.; Ben-Shalom, I. Y.; Brozell, S. R.; Cerutti, D. S.; Cheatham, T. E., III; Cruzeiro, V. W. D.; Darden, T. A.; Duke, R. E.; Ghoreishi, D.; Gilson, M. K. et al. *AmberTools18, part of AMBER 2018*; University of California: San Francisco, CA, 2018.
(85) Frisch, M. J.; Trucks, G. W.; Schlegel, H. B.; Scuseria, G. E.; Robb, M. A.; Cheeseman, J. R.; Scalmani, G.; Barone, V.; Petersson, G. A.; Nakatsuji, H.; Li, X.; Caricato, M.; Marenich, A. V.; Bloino, J.; Janesko, B. G.; Gomperts, R.; Mennucci, B.; Hratchian, H. P.; Ortiz, J. V.; Izmaylov, A. F.; Sonnenberg, J. L.; Williams-Young, D.; Ding, F.; Lipparini, F.; Egidi, F.; Goings, J.; Peng, B.; Petrone, A.; Henderson, T.; Ranasinghe, D.; Zakrzewski, V. G.; Gao, J.; Rega, N.; Zheng, G.; Liang, W.; Hada, M.; Ehara, M.; Toyota, K.; Fukuda, R.; Hasegawa, J.; Ishida, M.; Nakajima, T.; Honda, Y.; Kitao, O.; Nakai, H.; Vreven, T.; Throssell, K.; Montgomery, J. A., Jr.; Peralta, J. E.; Ogliaro, F.; Bearpark, M.; Heyd, J. J.; Brothers, E. N.; Kudin, K. N.; Staroverov, V. N.; Kobayashi, R.; Normand, J.; Raghavachari, K.; Rendell, A.; Burant, J. C.; Iyengar, S. S.; Tomasi, J.; Cossi, M.; Millam, J. M.; Klene, M.; Adamo, C.; Cammi, R.; Ochterski, J. W.; Martin, R. L.; Morokuma, K.; Farkas, O.; Foresman, J. B.; Fox, D. J. *Gaussian 16*, revision B.01; Gaussian, Inc.: Wallingford CT, 2016.
(86) Bayly, C. I.; Cieplak, P.; Cornell, W.; Kollman, P. A. A Well-Behaved Electrostatic Potential Based Method Using Charge Restraints for Deriving Atomic Charges: The RESP Model. *J. Phys. Chem.* **1993**, *97* (40), 10269−10280.
(87) Eastman, P.; Swails, J.; Chodera, J. D.; McGibbon, R. T.; Zhao, Y.; Beauchamp, K. A.; Wang, L.-P.; Simmonett, A. C.; Harrigan, M. P.; Stern, C. D.; Wiewiora, R. P.; Brooks, B. R.; Pande, V. S. OpenMM 7: Rapid Development of High Performance Algorithms for Molecular Dynamics. *PLoS Comput. Biol.* **2017**, *13* (7), No. e1005659.
(88) Martínez, L.; Andrade, R.; Birgin, E. G.; Martínez, J. M. PACKMOL: A package for building initial configurations for molecular dynamics simulations. *J. Comput. Chem.* **2009**, *30*, 2157−2164.
(89) McGibbon, R. T.; Beauchamp, K. A.; Harrigan, M. P.; Klein, C.; Swails, J. M.; Hernandez, C. X.; Schwantes, C. R.; Wang, L.-P.; Lane, T. J.; Pande, V. S. MDTraj: A Modern Open Library for the Analysis of Molecular Dynamics Trajectories. *Biophys. J.* **2015**, *109*, 1528−1532.
(90) Davison, A. C.; Hinkley, D. V. *Bootstrap Methods and Their Application*; Cambridge University Press: New York, 2005.
(91) Hsu, H.-P.; Paul, W.; Binder, K. Standard Definitions of Persistence Length Do Not Describe the Local "Intrinsic" Stiffness of Real Polymer Chains. *Macromolecules* **2010**, *43* (6), 3094−3102.
(92) Hsu, H.-P.; Paul, W.; Binder, K. Estimation of Persistence Lengths of Semiflexible Polymers: Insight from Simulations. *Polym. Sci., Ser. C* **2013**, *55* (1), 39−59.
(93) Almeida, L. E.; Borissevitch, I. E.; Yushmanov, V. E.; Tabak, M. Different Micellar Packing and Hydrophobicity of the Membrane Probes TEMPO and TEMPOL Influence Their Partition Between Aqueous and Micellar Phases Rather than Location in the Micelle Interior. *J. Colloid Interface Sci.* **1998**, *203* (2), 456−463.
(94) Hammouda, B.; Ho, D.; Kline, S. SANS from Poly(Ethylene Oxide)/Water Systems. *Macromolecules* **2002**, *35* (22), 8578−8585.
(95) Hammouda, B.; Ho, D. L.; Kline, S. Insight into Clustering in Poly(Ethylene Oxide) Solutions. *Macromolecules* **2004**, *37* (18), 6932−6937.
(96) Dormidontova, E. E. Influence of End Groups on Phase Behavior and Properties of PEO in Aqueous Solutions. *Macromolecules* **2004**, *37* (20), 7747−7761.
(97) Jacobson, H.; Stockmayer, W. H. Intramolecular Reaction in Polycondensations. I. The Theory of Linear Systems. *J. Chem. Phys.* **1950**, *18* (12), 1600−1606.
(98) Schäfer, L. *Excluded Volume Effects in Polymer Solutions: As Explained by the Renormalization Group*; Springer-Verlag: Berlin Heidelberg, 1999.
(99) Li, B.; Madras, N.; Sokal, A. D. Critical Exponents, Hyperscaling, and Universal Amplitude Ratios for Two- and Three-Dimensional Self-Avoiding Walks. *J. Stat. Phys.* **1995**, *80* (3), 661−754.
(100) Dittmore, A.; McIntosh, D. B.; Halliday, S.; Saleh, O. A. Single-Molecule Elasticity Measurements of the Onset of Excluded Volume in Poly(Ethylene Glycol). *Phys. Rev. Lett.* **9**, **2011***107* (14), 148301. .
(101) Rubinstein, M.; Colby, R. H. *Polymer Physics*; Oxford University Press: USA, 2003.
(102) Lee, H.; de Vries, A. H.; Marrink, S.-J.; Pastor, R. W. A Coarse-Grained Model for Polyethylene Oxide and Polyethylene Glycol: Conformation and Hydrodynamics. *J. Phys. Chem. B* **2009**, *113* (40), 13186−13194.
(103) Lee, H.; Venable, R. M.; MacKerell, A. D.; Pastor, R. W. Molecular Dynamics Studies of Polyethylene Oxide and Polyethylene Glycol: Hydrodynamic Radius and Shape Anisotropy. *Biophys. J.* **2008**, *95* (4), 1590−1599.
(104) Hsu, H.-P.; Binder, K. Stretching Semiflexible Polymer Chains: Evidence for the Importance of Excluded Volume Effects from Monte Carlo Simulation. *J. Chem. Phys.* **2012**, *136* (2), No. 024901.
(105) Oesterhelt, F.; Rief, M.; Gaub, H. E. Single Molecule Force Spectroscopy by AFM Indicates Helical Structure of Poly(Ethylene-Glycol) in Water. *New J. Phys.* **1999**, *1*, 6−6.
(106) Wang, S.-C.; Wang, C.-K.; Chang, F.-M.; Tsao, H.-K. Second Virial Coefficients of Poly(Ethylene Glycol) in Aqueous Solutions at Freezing Point. *Macromolecules* **2002**, *35* (25), 9551−9555.
(107) Tadokoro, H.; Chatani, Y.; Yoshihara, T.; Tahara, S.; Murahashi, S. Structural Studies on Polyethers, [-(CH2)m-O-]n. II. Molecular Structure of Polyethylene Oxide. *Die. Makromol. Chem.* **1964**, *73* (1), 109−127.
(108) Connor, T. M.; McLauchlan, K. A. High Resolution Nuclear Resonance Studies of the Chain Conformation of Polyethylene Oxide. *J. Phys. Chem.* **1965**, *69* (6), 1888−1893.
(109) Dahal, U. R.; Dormidontova, E. E. The Dynamics of Solvation Dictates the Conformation of Polyethylene Oxide in Aqueous, Isobutyric Acid and Binary Solutions. *Phys. Chem. Chem. Phys.* **2017**, *19* (15), 9823−9832.

https://dx.doi.org/10.1021/jacs.0c08709
J. Am. Chem. Soc. 2020, 142, 19631−19641